Article

Not peer-reviewed version

How to Cristallize a Glass with a Femtosecond Laser

Ruyue QUE , Matthieu Lancry , Maxime Cavillon , Bertrand Poumellec *

Posted Date: 24 April 2024

doi: 10.20944/preprints202404.1590.v1

Keywords: laser induced crystallization in glass; crystallization of oxyde glasses; femtosecond laser

 doi:10.20944/preprints202404.1590.v1

Article

How to Cristallize a Glass with a Femtosecond Laser

Ruyue Que, Matthieu Lancry, Maxime Cavillon and Bertrand Poumellec *

Université Paris-Saclay, CNRS, Institut de Chimie Moléculaire et des Matériaux d'Orsay, 91405 Orsay, France
* Correspondence: author e-mail address: bertrand.poumellec@universite-paris-saclay.fr

Abstract: Crystallization of glass through conventional thermal annealing in a furnace is a well-understood process. However, crystallization by femtosecond (fs) laser brings another dimension to this process. The pulsed nature of the irradiation necessitates a reevaluation of parameters for optimal crystallization and to understand the particularities in the case of using fs laser. This includes adjusting the laser pulse energy, the repetition rate, and the writing speed to either initiate nucleation or achieve substantial crystal growth. Therefore, a key challenge to this work is to establish reliable calculations for understanding the relation of the size of the crystallized region with respect to an ongoing transition (e.g., solid-to-solid, liquid-to-solid), and accounting for the aforementioned laser parameters. In this context and based on previous work, we simulate a temperature distribution (in space and time) to model the thermal treatment at any point in the glass. By setting the condition that the temperatures are between the glass transition and melting temperature, we can deduce the crystallized region size to be compared with experimental observations. For that purpose, the knowledge of the beam width at the focal point and of the absorbed beam energy fraction are critical inputs that were extracted from experiments found in the literature. After that, management of the crystallization process and the width of the crystallization line can be achieved according to pulse energy e.g. crystallite size, and also the effect of the scanning speed can be understood. Among the main conclusions to highlight, we disclose the laser conditions that determine the extent of the crystallized area and deduce that it is never interesting to increase the pulse energy too much but rather the repetition rate for uniform crystallized line.

Keywords: laser induced crystallization in glass; crystallization of oxyde glasses; femtosecond laser

1. Introduction

3D localized crystallization in glasses brings interest as it introduces the possibility to precipitate crystalline phases that present optical nonlinear, ferroelectric, or pyroelectric, properties. For example, it leads to formation of non-center-symmetric crystals in optically suitable glasses [1]. This approach underscores that crystallization, a thermo-kinetics process [2,3], is influenced by temperature (and time), occurring between the glass transition temperature (T_g) and the melting temperature (T_m) of the given precipitated phase(s), and dictating nucleation and growth rates. While spatially selective crystallization using a femtosecond laser has been extensively demonstrated in various glasses [1], this process appears more complex than using a continuous-wave (CW) laser, arising from the pulsed nature of the laser (up to several MHz), and its high peak intensity triggering nonlinear processes. For example, in lithium niobium silicate glasses (LNS) [4], crystallization patterns of the $LiNbO_3$ phase strongly depend on pulse energy or laser polarization.

While some physical aspects of the crystallization mechanisms have been understood, we aim to further explain and predict semi-quantitative aspects, particularly the correlation between laser parameters and specific optical or material properties. A goal is to minimize the number of experiments by performing calculations that facilitate a selection of relevant parameters to induce crystallization. For this purpose, we build upon a simple analytical solution developed in a previous work ([5], chapter 2), to physically describe the thermal dynamics induced by pulsed laser absorption and subsequent transformations.

 doi:10.20944/preprints202404.1590.v1

In this work, we first simulate the evolution of the temperature distribution induced by a pulsed fs laser. Once the temperature modulation is known, it can be combined with time – temperature - transformation (TTT) diagram) for crystallization. The temperature calculation relies on modelling the energy source as spherical, and requires knowledge of several parameters:

1) the ratio (labelled R_τ) between the pulse period ($\tau_{RR} = 1/RR$, with RR being the pulse repetition rate) and the heat diffusion time ($\tau_D = w^2/4D_{th}$, w being the light beam waist radius at $1/e$ at the focus, and D_{th} the heat diffusion coefficient or diffusivity). While R_τ depends thus on w, the latter usually in not reliably known due to the complexity of non-linear effects in the light-matter interaction. For this purpose, we performed a compilation of values extracted from literature permitted to clarify its dependency on the incident pulsed laser energy (Please refer to Appendix 1).

2) the fraction of the incident energy effectively absorbed by the material (labeled A). Absorption primarily occurs through nonlinear absorption (multiphoton ionization). Plasma reflection or scattering is also expected, reducing the coefficient A. After absorption of a small part of the pulse energy, the absorption becomes linear due to limitations of the electron plasma density [6] by a balance of multistep absorption, trapping, electron-electron or electron-phonon collisions. Given the lack of precise information about all these processes, extracted values from the literature (reported in appendix 2) enables one to set A values. As one is not aware about that, A is a function of the incident pulse energy, the pulse duration, and the material composition.

Another problem more specific to crystallization is the location of the crystallization domain in the TTT diagram in the confined condition of the tightly focused fs pulsed laser. Indeed, the specificities of the process may change the limit of the crystallization domain compared to the classical one [7–9]. Due to these uncertainties, we tested our approach using LNS glasses for laser conditions employed in [4,10,11] for which these aspects are relatively well known.

Paper is organized in such a way that following a brief recall on classical crystallization process (section 2), and temperature calculation from specific hypothesis (section 3), we are describing how the crystallization process behaves, firstly, within heat accumulation regime (later defined, see Section 4) and, secondly, without heat accumulation, see section 5, large temperature oscillations). Finally, we compare the results from the approach with respect to several experimental values according to pulse energy and scanning speed (section 6) and draw conclusion -1- about optimization of laser parameters, -2- that the width of crystallization area can be understood -3- that incident light energy fraction may change with the number of pulses.

2. Basic: Brief Recall on the Crystallization Process

The appearance of crystals in glass is a two-step process: nucleation and growth [2,9]. Crystallization is generally growth-limited at low temperatures and nucleation-limited at higher ones. Moreover, the domain of crystallization is defined from a TTT diagram [9]. It collects the time (called incubation time) requested at a given temperature to observe a first seed. This diagram, generally established for isothermal treatment, takes the time origin (t = 0) when the sample is in the condition to crystallize for a given temperature. This temperature is comprised between T_g and T_m. A boundary can be plotted in this TTT diagram delimitating the appearance of typ. 10^{-6} part crystallized in the glass volume (thick black line in Figure 1). The position of the crystallization domain in the TTT diagram is dependent on the treatment pathway. For example, its position will be shifted if the temperature is continuously decreasing (or not) from T_m [12]. In that case, the growth is delayed because the nucleation is slowed down. But for the purpose of this paper, we will ignore this and simply consider the thermal treatment curve experienced by the material at a given spatial position with coordinates $\alpha_0, \beta_0, \gamma_0$. The time-temperature applied to this position ($T(\alpha_0, \beta_0, \gamma_0, t)$). This function of time is simply obtained by the displacement of the temperature distribution function (the variation of the temperature in space) in the static case. This approximation is valid for speed smaller than the diffusion speed ($2D_{th}/w$, typ. a few cm/s). As we recalled above, the thermal treatment should exhibit temperatures in the T_g to T_m range. However, heating a material using a pulsed laser, resulting in oscillatory temperature in volume, and impacted by non-linear optical processes, is a complex problem that prevents to easily draw conclusions for managing the process. The important aspect of

 doi:10.20944/preprints202404.1590.v1

solving this issue is to take into account the effect of these parameters while preserving the main physics associated to the induced transformations. Consequently, we have developed in [13] a simplified approach for understanding how $T(\alpha,\beta,\gamma,t)$ is changing according to the laser parameters (pulse energy, pulse repetition rate, beam scanning speed, beam width and material properties).

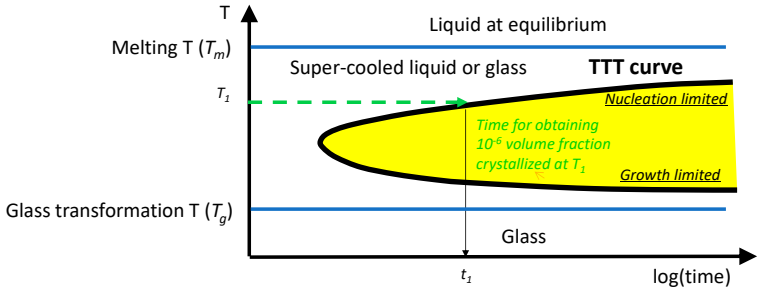

Figure 1. Crystallization domain in a Time – Temperature – Transformation (TTT) diagram (in Yellow). Its boundary is black. The glass and melting T is deep blue. T_1 is an example of isothermal treatment that leads to the incubation time t_1 for beginning to crystallize.

3. Temperature Distribution and Its Evolution during Laser Writing

The 3D Fourier equation with a spherical energy source at the focal volume assuming a tightly focused laser beam and temperature independent physico-chemical properties is employed. Usually, for 3D direct laser laser writing, the focusing objective NA is above 0.5. This section is mostly didactic from what has been already published in [13]. The approximation taken into account are that we consider a pulse duration such that the thermal diffusion is not yet active, i.e., << 0.1 µs and a scanning speed (v) much lower than the diffusion speed (typ. few cm/s). Consequently, the shape of the spatial temperature distribution is not time dependent, the only time dependence is introduced by the beam scanning taken in the α direction and appears as $\alpha+v.t.$. β and γ are fixed at the position α_0 and γ_0, with γ direction corresponding to the beam propagation axis. The scanning speed (v) defines the pulsed number deposited punctually as $N_p = 2w.RR/v$. The laser pulse energy E_p defines the maximum temperature increment T_{00}, introduced by a single pulse above an initial temperature T_{init}: $T_{00} = \frac{A \cdot E_p}{\pi^{\frac{3}{2}} \rho C_p w^3}$ with A the fraction of absorbed energy (previously defined), ρ and C_p are the glass density and heat capacity, respectively. Additionally, a normalized radius $r_w=r/w$ is defined, with r being a radial distance from the center of the beam focus.

All calculated temperatures are normalized with respect to T_{00}, as follow:$T_{norm} = (T-T_{init})/T_{00}$. T_{norm} is oscillating at $1/RR$ period at any distance from the focus center. This temperature oscillation is comprised between a maximum (T_{max}) and a minimum (T_{min}), which varies according to the laser irradiation conditions. After a sufficient number of pulses, both T_{max} and T_{min} reach a steady state regime. Achieving this steady state regime is dictated by the ratio R_τ as previously defined and taking the form $R_\tau = 4D_{th}/RR\ w^2$. For instance, for large R_τ values (i.e. >16 for $T_{min}<0.03T_{max}$) the pulse contributions are independent of each other whereas for smaller R_τ values (<16), heat accumulation from pulse to pulse contribution begins to appear (and thus T_{min} *overcomes* $0.03T_{max}$).

N_{SS} corresponds to the minimum number of pulses necessary to reach the steady state regime. Its expression is given in eq.A4 in Appendix 3. This calculation can be performed either for T_{min} and T_{max}.

The temperature spatial distributions of T_{max} and T_{min} (normalized in the form of T_{norm}) for various R_τ values are provided in Figure 2. When R_τ is small (large RR or small diffusivity), T_{min} and T_{max} have no large relative difference compared to their average values because the oscillation amplitude is always limited to $\exp[-(r_w)^2]$ whereas T_{max} and T_{min} amplitude is converging to $2/R_\tau$ at the beam center but converges to $\frac{\sqrt{\pi}}{R\tau.r_w} erf(r_w)$ elsewhere on heat accumulation. When this situation can be reached, the pulse energy can be adjusted to compensate for a RR increase. It is also worth to note that, when R_τ decreases, the shape of the curve converges to $erf(r_w)/r_w$ curve (see Eq. A6

 doi:10.20944/preprints202404.1590.v1

Appendix 4). It results that the temperature distribution decreases much slower for the radius increasing than a gaussian one. This last shape is the shape of the energy source and of the temperature distribution for the case where R_τ is large. Note that in the case of heat accumulation, the overhal maximum temperature (at the center of the beam actually) is defined by $A.E_p.RR$ i.e. roughly the average incident power.

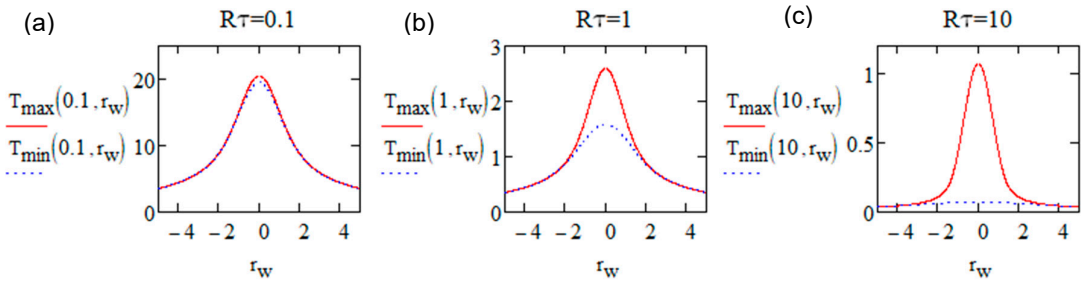

Figure 2. Spatial distribution of T_{min} (blue dash, by Eq.A3) and T_{max} (red, by Eq.A1) in the normalized form (see text) and as a function of the reduced radius r_w when (a) $R_\tau = 0.1$, (b) $R_\tau = 1$ and (c) $R_\tau = 10$.

For large R_τ values, corresponding to small RR and / or large D_{th}, the oscillations are relatively large as pulse contributions are separated and thus T_{min} appears to have small values (See Figure 2c). If we consider negligible being T_{min} smaller than 3%.T_{max} then $R_\tau > 16$ (for smaller than 6%.T_{max} then $R_\tau > 7$. For $R_\tau > 10$, T_{min} is smaller than 4.4%T_{max}). This defines the limit of the domain of heat accumulation. The increase of R_τ (Figure 2a to 2c) clearly show that the shape of T_{max} is also converging with increasing R_τ to the shape of the beam energy distribution (a gaussian beam, with an envelope having a spatial distribution following $exp[-(r_w)^2]$), therefore and in the limited case becoming independent on R_τ. The maximum absolute temperature at the center is T_{00} in this case. It is defined by E_p only (independent of R_τ and so especially on RR)

For intermediate R_τ values, exemplified in Figure 2b-c, the temperature oscillations are limited between T_{max} and T_{min}. This is shown with particular cases with energy source volume as a shoe box in [14] for $R_\tau = 2\ and\ 20$ or in [15] for $R_\tau = 20$.

But, in this paper, we specify that when r_w>2, the difference between T_{min} and T_{max} is vanishing as seen in [16].Therefore we can deduce in what conditions of r_w and R_τ, the temperature oscillations can be neglected and the use of an average temperature T_{mean} might be applicable (Appendix 3 Eq.6-8).

Another important point for this current work is the dependence of the full width at half maximum (FWHM) of the temperature distribution with respect to R_τ. Its variation is less than a factor 2 in the relative radius scale (r_w). In fact, the largest change is at the pedestal of the distribution.

4. Case of Low R_τ Values (High *RR* or Low D_{th}) i.e. within Heat Accumulation Regime

Here, R_τ is such that it is much smaller than 10 e.g. R_τ=0.1, due to the use of large repetition rate or a weakly thermally diffusing material. R_τ=10 is the limit for T_{min}=4.4%T_{max}., corresponds to T_{min} very close to T_{max}. In that case, a pulse contribution has no time to vanish significantly before a next pulse absorption induced another temperature increase. It is the case of heat accumulation and the behavior is like the one for Continuous Wave (CW) lasers.

In this section, we deal with conditions where the pulse number received punctually (Np as defined earlier) is above the number of pulses required to reach the steady state (N_{ss}). This situation yields to two possibilities for which the temperature is higher than T_g : i) the temperature remains lower than T_m, and ii) the temperature overcomes T_m for some distance from the center of the beam focus during the thermal treatment. Each situation is described below.

i) **Moderate *Ep* leading to a temperature lower than T_m**

Preprints.org (www.preprints.org) | NOT PEER-REVIEWED | Posted: 24 April 2024 doi:10.20944/preprints202404.1590.v1

To describe the temperature evolution and for illustration purposes, we set the laser parameters so that the temperature values fall within acceptable temperature interval. In this section, we took for the moment as example T_g = 579°C coming from the physico-chemical properties of LNS glass and T_m = 1257°C (T_m is the melting temperature of the formed $LiNbO_3$ crystals in LNS). Additional data requested for the calculation, are provided in the table in Appendix 3. Therefore we used low absorption fraction (A) and pulse energy (E_p) to low values, provided in the caption of Figure 3. The beam width at *1/e* has been fixed to a "reasonable value" for such small pulse energy, i.e., w = 1µm. In this condition, similar to Figure 2a, the oscillations (eq. A2 in Appendix 4) are small enough to be neglected. This can be observed in Figure 3, rendering T_{mean} a valid approximation if requested.

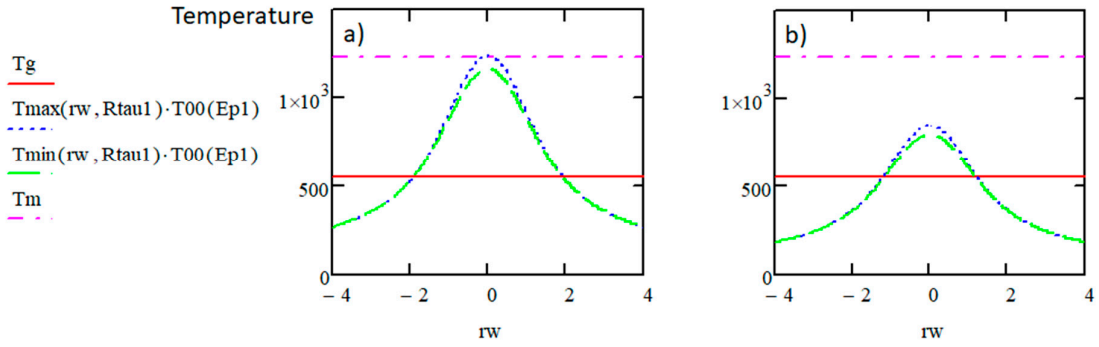

Figure 3. Temperature distribution for T_{max} and T_{min} with respect to the normalized radial distance r_w for $R_\tau = \frac{4D_{th}}{RR}w^2$ (called Rtau1 in the figures of this paper) = 0.13, A = 0.1, w = 1.65µm, RR = 300 kHz, Ep (called Ep1 in the figures of this paper) = 54 nJ for (a) and 37 nJ for (b), T_g and T_m, shifted by room temperature, are also shown. T_{max} *and* T_{min} is calculated from eq. A1 and A3 in Appendix 4.

Then, the temperature distribution is transformed into time domain to obtain thermal treatment curves (Figure 4b-c, T-t dependency) replacing the static normalized radius r_w by the coordinate of the place we are looking at in the moving material r_{wd}, taking the beam center as a reference(see Figure 4a). The relative position in the beam of this point is related to relative time from the following relation: $r_{wd}(t, v, d, \beta) = \sqrt{(v.t/w + d)^2 + \beta^2}$. Then, the time origin of the treatment for crystallization is defined when T starts to overcome T_g. This occurs at a distance d from the center of the temperature distribution i.e. at an abscissa d dependent on β(distance from the line axis) i.e. $d^2 = {r^0_{wdg}}^2 - \beta^2$. r^0_{wdg}, the radius of the isotherm T_g, is then obtained by solving $T_{mean}(r^0_{wdg}, R_\tau)=T_g/T_{00}$ where T_{mean} is an average temperature defined in appendix 4 eq. A6. r^0_{wdg} is the also the maximum width of the crystallized region.

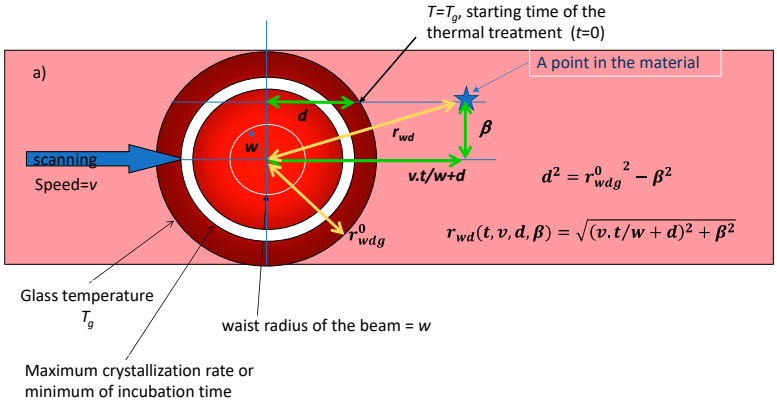

 doi:10.20944/preprints202404.1590.v1

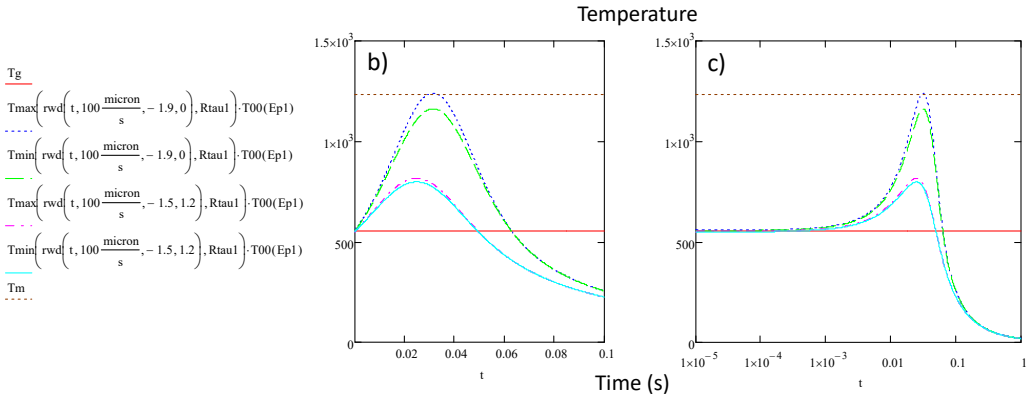

Figure 4. Plot of the treatment curves in the time scale from the time when the temperature overcomes T_g a) scheme for illustrating the various normalized distances used in the calculation of the thermal treatment curve, b) treatment curve at the center $\beta = 0$ or at $r = 1.2w$ ($\beta = 1.2$). c) same as (b) but showing the time in log scale. $A = 0.1$, $w = 1.65$ µm, $R_\tau = 0.13$, $E_p = 54$ nJ. v = 100µm/s. The thermal treatment of the point at coordinates 0,0,0 begins when the temperature overcomes T_g, here when the beam center is distant by $1.9w$ (third parameter in rwd), whereas, it begins later, at $1.5w$, for a point in the periphery of the line at coordinates 0,1.2,0.

Figure 4 display a time-temperature thermal treatment. Therefore, provided that the crystallization domain is known (TTT diagram, see above) the scanning speed must be adjusted to ensure the thermal curve intersect with the crystallization domain as in Figure 5 at speed $v1$ or $v2$. For the speed higher than v_{lim}, the curve does not touch the domain anymore and the crystallization is not possible. We see also that for speed $v1$, crystallization starts from bottom side of the domain and then crossed it and is thus not limited in growth. However, if T_{max} is not so large ($T_{max} < T_m$), the growth can be controlled. For $v2$, crystallization starts from the growth side and is sensitive to the pre-existence of nucleation seeds.

It is also important to note that r^0_{wdg} is in principle larger than the half-width of the crystallized region. Indeed, r^0_{wdg} is a circle where t=0, but the crystallization occurs eventually after some incubation time that could be longer than at the center, due to the T_{max} decrease when going to the line edge. This contributes to a narrowing of the line but this effect is small as shown in [17] Figure 4, we see that at the speed limit, the width is not vanishing. The disappearance of the crystallization is thus arising from the process described in Figure 5. The width of the crystallization area is weakly sensitive to the scanning speed for a solid to solid transformation. This valid the criterion on T_g and T_m used in our approach.

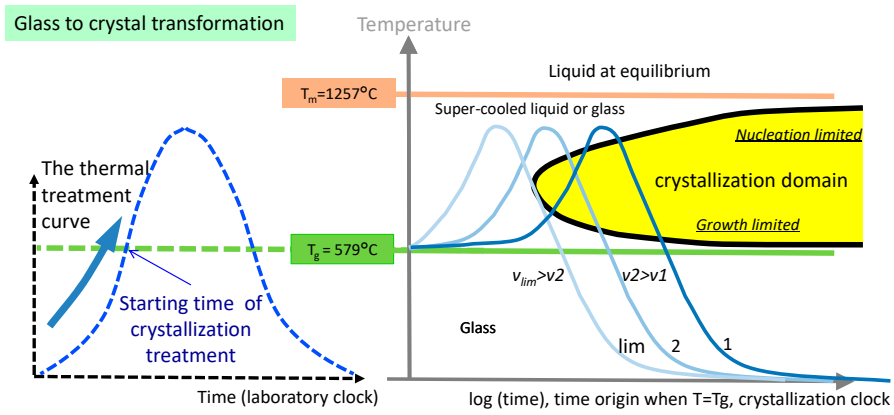

 doi:10.20944/preprints202404.1590.v1

Figure 5. Show of position of the treatment curve versus the crystallization domain in the case of solid glass to crystal transformation (T_g<T<T_m).

ii) At the periphery of the line (e.g. for β=1.2 in Figure 4), the temperature is smaller than the one at the center, but the crystallization condition remains somewhat similar : the treatment curves cross the crystallization domain almost at the same incubation time. From this view, the results are rather intuitive. First, a lower scanning speed would lead to a larger crystal growth. Second, there is a minimum laser power ($P = E_p.RR$) necessary to overcome T_g, with a maximum scanning speed necessary for the thermal treatment curve to cross the crystallization boundary. As the power increases, the speed limit increases until the maximum in space of the average temperature reaches T_m. Beyond this point, the crystallization process is different, and is the topic of the next section. Large E_p yielding temperatures overcoming T_m. In this case, if crystallization occurs, it starts from the liquid phase, with the system potentially crystallizing as the temperature decreases below T_m. Similar to previous situation, d(β) is defined by $d^2 = {r^0_{wdm}}^2 - \beta^2$. r^0_{wdm}, which is the radius of the isotherm T_m, (i.e. a circle with a radius smaller than the one for T_g), is then obtained by solving the following equation that includes T_m:.$T_{mean}(r^0_{wdm},R_\tau)=T_m/T_{00}$. r^0_{wdm} is also the maximum size of the melted region. We have $\beta<r^0_{wdm}$, dashed blue curve in Figure 6. When $r^0_{wdm} < \beta < r^0_{wdg}$ (green curve), the results of section 4i apply. Then, the scanning speed should be adjusted to ensure the treatment curve to reach the crystallization domain. We see that in this case, entry into the crystallization domain is necessarily from the top side (nucleation limited). It is sensitive to the side stimulation because the side has crystallized before.

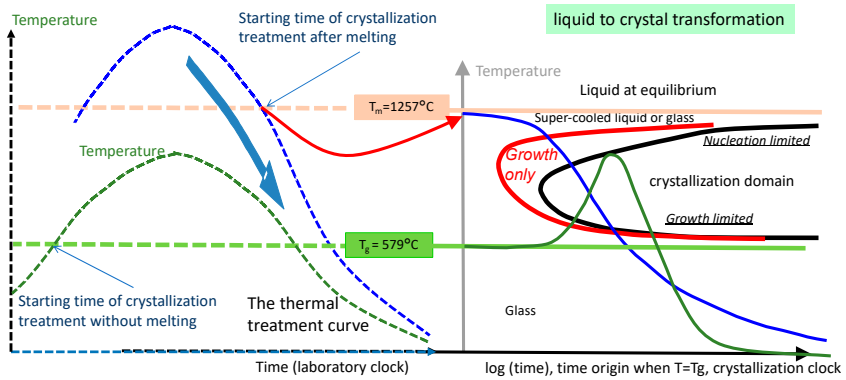

Figure 6. the position of the treatment curve versus the crystallization domain when a part of the trace is melting i.e. a liquid to crystal transformation. The region delimited by red one is for growth only.

5. Case of High R_τ Values (Low RR and Large D_{th}) i.e. Out of Heat Accumulation Regime

Here, R_τ is such that it is larger than 10, due to the use of small repetition rate or a strong thermally diffusing material. In that case, a pulse contribution has enough time to vanish significantly before a next pulse absorption arrival. There is no heat accumulation but as we can see in Figure 2c, this is true only for $\boldsymbol{r_w}$ smaller than approximately 3. For the periphery of the heat affected region, there is a smoothening of the temperature oscillations due to heat diffusion.

On the contrary, for smaller reduced radius, T_{min} is close to zero, and the temperature oscillates between T_{min} and T_{max} during each period. Assuming that the pulse number received punctually (N_p) is above the pulse number to reach the stationary state (N_{ss} formula eq.A4 Appendix 4), we can simulate the temperature oscillations at the steady state simply. Note that the oscillation at this stage

 doi:10.20944/preprints202404.1590.v1

is due to a series of pulse contributions collected in the function $T_{osc}{}'(r_w, x, R_\tau)$ where x (between 0 and 1), is the temporal position in the period and is thus the floating value of $t.RR$. The simulation function of the temperature called *SimpulseT* is $SimpulseT(r_{wd}(t,v,d,\beta),R_\tau,E_p)/T_{00}(E_p) = T_{min}(r_{wd}(t,v,d,\beta),R_\tau) + T_{osc}{}'(r_{wd}(t,v,d,\beta),x(t,RR),R_\tau)$ (see eq A9 appendix 4) with r_{wd} defined as in the previous section and related to the time origin for crystallization according to one of the two cases for which the temperature is above or below the melting temperature T_m.

i) Moderate E_p such that the temperature is not overcoming T_m

As we can see in Figure 7, the punctual thermal treatment is beginning when $T_{max}.T_{00}$ is overcoming the melting temperature for the first time during the scanning. The relative position in the beam is translated in relative time from the following relation$r_{wd}(t,v,d,\beta) = \sqrt{(v.t/w+d)^2+\beta^2}$: $d(\beta)$ *defined by* $d^2 = r_{wdg}^{0\ 2} - \beta^2$with r_{wdg}^0 solution of $T_{max}(r_{wdg}^0,R_\tau)$=$T_g/T_{00}$.

However, the existence of oscillations between T_{min} and T_{max} are such that there are dead times, defined as the time for which the temperature decreases below T_g. Consequently, the efficiency, taken as the ratio between the active time (during which $T_g<T<T_m$) and the thermal treatment time, is much smaller than one. This is different from small R_τ values; again for which T_{max} is close to T_{min}, and a T_{mean} can be employed.

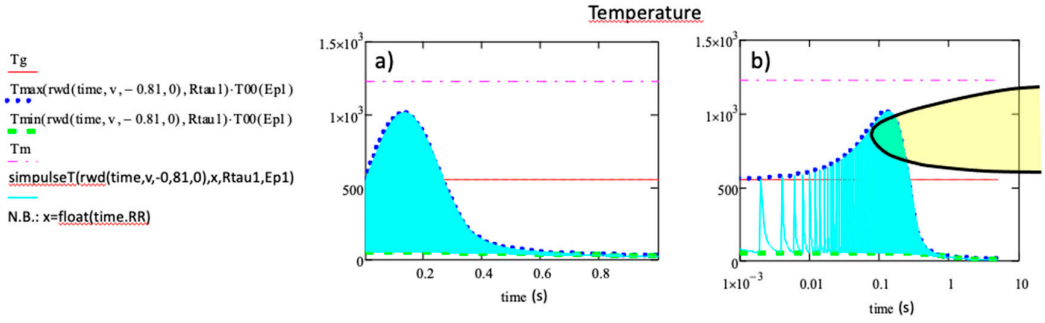

Figure 7. Thermal treatment curve (T_{max}, T_{min}, *SimpulseT*) for a point at the center (0,0,0) of the written line. R_τ = 13, A = 0.15, w = 1.65 µm, E_p = 0.5 µJ, 100 kHz, v = 10µm/s, (RR is fixed to 400 Hz just for illustrative purpose). time is in a) linear and b) log scale.

The time for which crystallization is possible (as per the definition of efficiency before) is computed by solving the following equation: $SimpulseT(r_w,x,R_\tau)$=T_g. This gives the temporal interval $x1$, $x2$ graphically defined in Figure 8a during the pulse period and for which the temperature is above T_g according to r_w i.e., the normalized distance to the beam center.

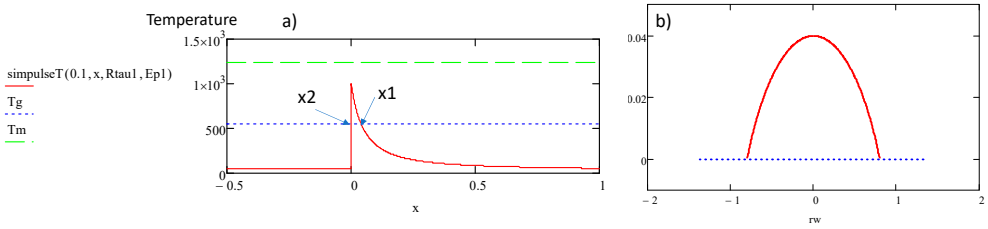

Figure 8. a) positions x1, x2 in the pulse period, between which the temperature is above T_g, b) the efficiency (definition in the text) as a function of r_w, x1 red curve, x2 dashed blue curve. Same laser parameters as in Figure 7 are used..

As we can see in Figure 8b, the efficiency of the thermal treatment (defined as $x1$-$x2$) is a function on the distance of the position away from the beam center (r_w). This reduction of the efficiency means that to reach crystallization around the periphery of the beam, the scanning speed must significantly be decreased. In fact, in those conditions, the thermal treatment time is much smaller than the irradiation time. We also pinpoint that beyond some departure from the center (e.g. here β> 0.7, i.e.,

 doi:10.20944/preprints202404.1590.v1

in the direction perpendicular to the scanning direction, with the parameters used in Figure 7), the crystallization is no more possible from kinetics reason ($T<T_g$). This r_{wdg}^0 defines the maximum width of the crystallization region.

ii) Large E_p such that the temperature is overcoming T_m

In that case, a new treatment begins when a pulse oscillation is decreasing below T_m assuming that material melted before.

The use of *SimpulseT* function is valid. Using this expression, we detect the position in the period (*x3* in Figure 9a) for which the temperature has overcome T_m and returns below it. This position is the starting time for thermal treatment that ends at position *x1*. But if a next temperature pulse induces temperature overcoming T_m, as the material is expected to melt and thus lost its memory, there will be a new time origin to compute from this next pulse. So, the last pulse defines the beginning of the treatment that goes on afterwards, i.e. when T_{max} is decreasing below *Tm* in the course of the scanning. This is obtained by solving $SimpulseT(r_w,x,R_\tau)=T_m$. This yields positions *x3* and *x4* in the period as shown in Figure 9b.

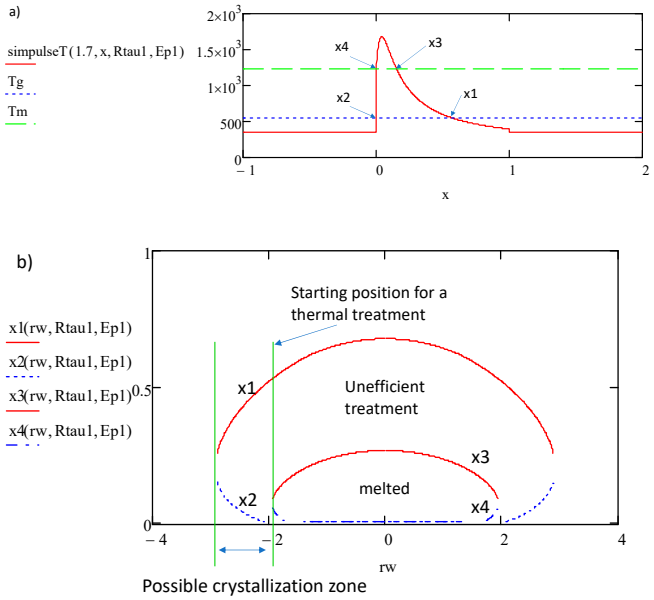

Figure 9. Values of *x* for the crossing points according to the distance from the beam center r_w. a) : definition of the remarkable temporal locations in the period. x1 and x2 where the temperature equals the glass one, x3, x4 where it equals the melting one, b) : variation of the remarkable temporal locations according to the distance from the beam center. The part of the heat affected region where crystallization is possible is also indicated. This computation has been achieved with E_p = 5µJ, w = 1.65 µm, A=0.2, RR = 60kHz, $R_\tau = 22$.

As we see in Figure 9, just a part of the pulse is "active" to induce crystallization (x2-x1<1) and just a part of the temperature distribution is also possible. Following the picture in Figure 9b, only the tail of the temperature distribution is used. When T is no more overcoming T_m, and as shown in Figure 10 with d=1.92 for β=0, *x3* and *x4* do not exist anymore and until *x1* and *x2* still do, the temperature is overcoming T_g.

 doi:10.20944/preprints202404.1590.v1

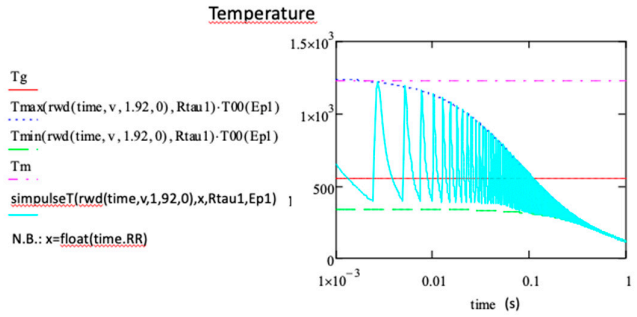

Figure 10. Temperature evolution over time when pulses has overcome T_m corresponding to a liquid to solid transition. The last pulse contribution that does not overcome T_m defines the time origin. Computation is made with parameters of Figure 9 with a scanning speed of 15µm/s.

From the Figure 9a above, it can be noticed that the efficiency for crystallization is again smaller than 100% and that the writing speed must be decreased to trigger the crystallization. Regarding the sides of the line ($\beta \neq 0$), the maximum of T_{max} is decreasing with y and the process described here will stop when T_{max} will not overcome T_m anymore ($r_{wdg}^0 < \beta < r_{wdm}^0$). For these β, the situation is the same as the one described at the beginning of this section. The transition is solid-solid and starts from the front of the T distribution i.e. before the line center (in reference to the laboratory clock).

6. Application to the Case of LNS Glass

The next section is dedicated to applying the above findings to an experimental case using LNS glasses. The objective of this section is to show how the width of the thermally transformed region is linked to the laser parameters especially to the pulse energy. It is based on real case for which the beam waist and fraction of absorbed pulse energy (A in T_{00} expression, equation A10 Appendix 4) are crucial information, believed much smaller than we show in this paper. After data analysis from different authors, we have pointed out that the dependence on pulse energy of the beam waist w is not very sensitive to the material when comparing silica and LNS family (Appendix 1). On the contrary, the pulse energy dependence of A (appendix 2) is sensitive to the pulse duration and to the material. Therefore, the methodology in this section is to start with the pulse energy, the numerical aperture, and the pulse duration, to show that 1- the beam waist and the fraction of absorbed energy can be defined with enough accuracy for the purpose of this paper, and 2-. then with these quantities and their dependence with the laser parameters established reliably enough, to draw conclusions on the laser induced crystallization process.

We start from low pulse energy (0.5-1 µJ). The experimental half width of crystallized area is measured to be 1.65 µm (using 0.7 µJ in [4]) with the following laser parameters: wavelength 1030 nm, pulse duration 300 fs, RR = 300 kHz, NA = 0.6, v = 5 µm/s [4]. With these values, we know that solid-solid transformation (crystallization, ref [4]) occurs. On the other hand, the presence of nanogratings [18] indicates the size of the laser beam as these structures are only created by light. We deduce that w = 1.65 µm. However, we have to adjust A. There are different processes that contributes to this fraction. The first one is the reflection of light (from Fresnel, or from the electron plasma mirror that is formed by the electron excitation in conduction band or also some light scattering). The second one is that if a part is absorbed, a part is also transmitted as the absorption is never total in transparent materials with non-linear absorption. Since the modification is a solid-solid transformation, the temperature does not overcome T_m (as shown in the previous sections), and the value of A has to be smaller than 0.09 for 0.7 µJ. This value falls within the values found in the literature and presented in Appendix 4 Figure A2. Once all of these parameters are known, the simulation can be carried out similarly as presented in the previous sections.

 doi:10.20944/preprints202404.1590.v1

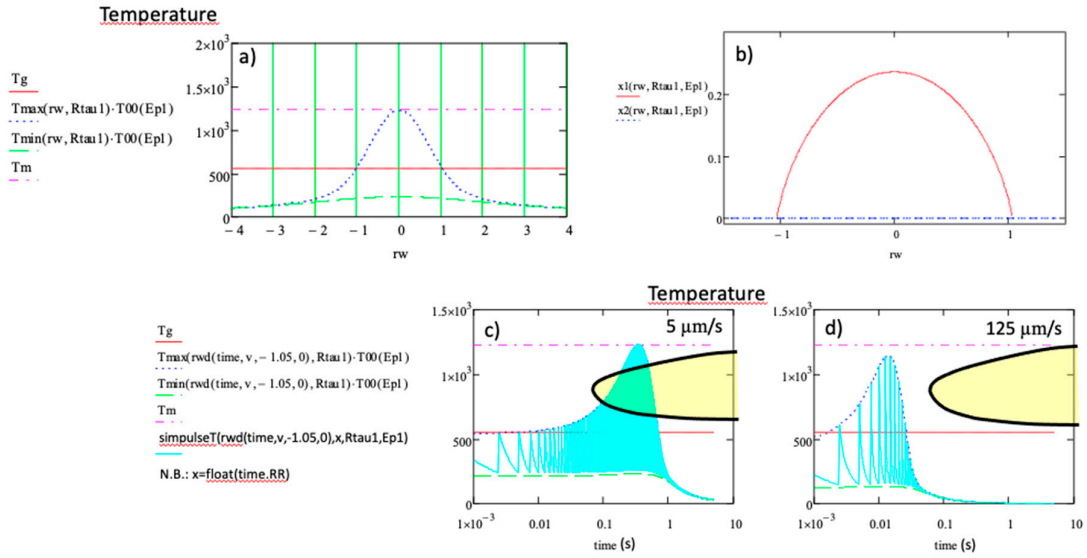

Figure 11. temperature simulation in LNS glass for E_p = 0.7µJ, A = 0.09, w = 1.65 µm, R_τ= 4.4, scanning speed=5 µm/s for a, b and c., a) : T_{max} and T_{min} distribution, b) : useful part of the T oscillations c) : corresponding treatment curve for v = 5 µm/s, d) the same with v = 125 µm/s.

The results are summarized in Figure 11 and below:

- The possible crystallization would fall within a fraction of second for v = 5 µm/s provided that the efficiency was 100%, but this is obviously not the case. On the contrary, the maximum efficiency is 22% here (see Figure 11b). The real treatment time is thus (x1-x2) multiplied by the time scale of the Figure 11c. On the other hand, as crystallization is actually observed in LNS for v up to 125µm/s [17] in a 0.5-1 µJ interval, 1030 nm, NA = 0.6, τ_{RR} = 250 fs, RR = 200 kHz, w = 1.6 µm (for which the steady state is reached). This leads to position the crystallization nose in the time range of 10 ms, i.e. an order of magnitude lower than the isothermal treatments in conventional furnace, in large volume without stress field [11].
- The calculated crystallized half width is close to the beam waist one, with the criterion that the temperature should be above T_g. We conclude that there is almost no line broadening originating from the thermal effect for this pulse energy as it is experimentally observed.

Now, and based on the above discussion, one can wonder how does width evolve when E_p is increased. To answer this aspect, we will deal with two distinct examples, at low and higher pulse energies.

First example: We know that solid-solid transformation occurs until 1.0 µJ and that for higher pulse energy, a part of the crystallized region originates from a liquid to solid transformation. For instance, let us consider the pulse energy 1.3 µJ. For this value, the half width of the crystallized region is 3.73 µm. We can measure the laser beam radius from [4] reported in Figure A1 at 2.6 µm. R_τ is thus decreases from 4.4 to 1.8 with the pulse energy increase. The indirect variation of R_τ with the pulse energy was not expected. It pushes the system to be in heat accumulation regime even if RR is constant. Additionnaly, A increases itself to 0.15. Using these data, the computation is summarized in Figure 12.

 doi:10.20944/preprints202404.1590.v1

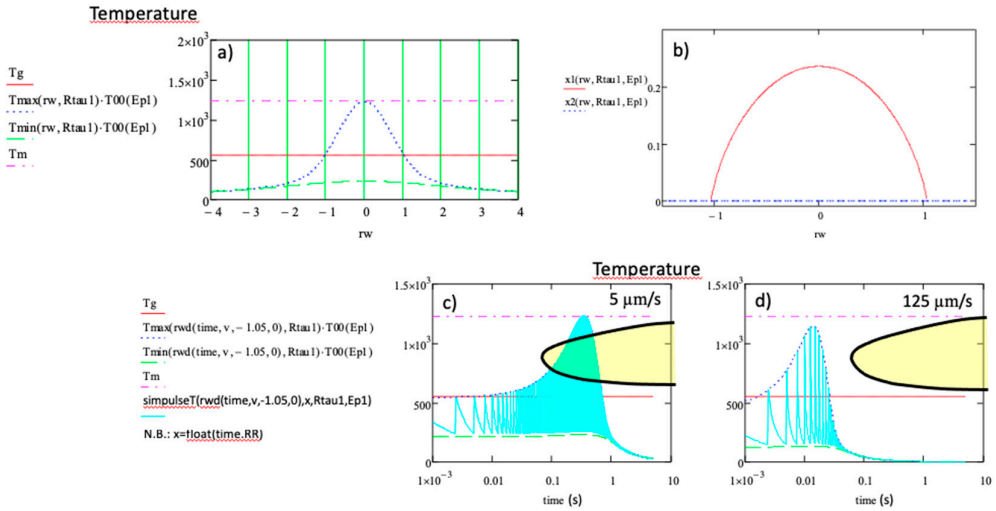

Figure 12. Temperature computation in LNS glass for Ep=1.3 µJ, w=2.6 µm, A=0.15, R_τ=1.8. Laser parameters : λ=1030nm, τ_p=300fs, RR=300kHz, NA=0.6,v=5 µm/s. a) T distribution, b) efficiency c) simulation on time.

The provided results indicate that

- The efficiency is close to 100% due to the effect of heat accumulation that increases T_{min} above T_g.
- The calculated crystallized radius is found to be at 1.25w. There is thus a small broadening of 25% compared to the beam waist w. There is thus a crystallized part that is not submitted to the beam where there is no submicrostructuring induced by the laser light. There is also a melted region smaller than the beam waist (half width = 0.48w). We see also that there is no obvious correlation between the beam width and the melted region.

For completeness, another experimental result available for 1.8 µJ has been computed and reported in the Table 1. It shows reasonable agreement with the experimental results.

Second example: considering much higher pulse energy, let's say 4.2 µJ as used by Veenhuizen et al. [10], with laser parameters as follows 175fs, 200 kHz and varied scanning speed v. The authors of the aforementioned reference observed a crystallization full width of 31.3 µm for 15 µm/s and 9.82 µm for 75µm/s i.e. a significant variation. From Figure A1 in Appendix 3, w seems to be around 4.5 µm and thus R_τ=0.9, A can be evaluated to 0.32 from Figure A2 in Appendix 4. Results are shown in Figure 13.

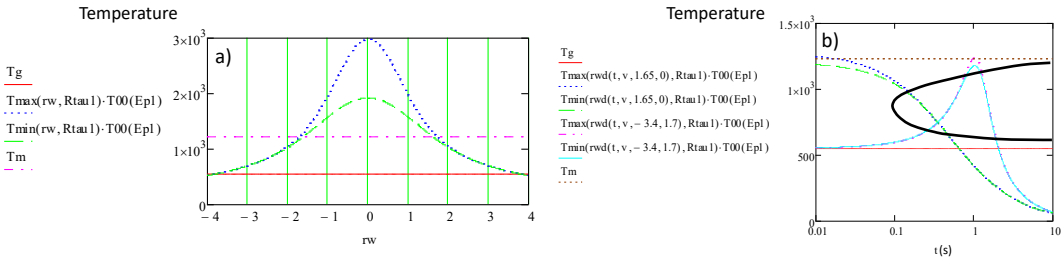

Figure 13. Temperature computation in LNS glass for Ep=4.2 µJ, w=4.5 µm, A=0.32, R_τ=0.9 Laser parameters : λ=1030nm, τ_p=300fs, RR=200kHz, NA=0.6, v=5 µm/s. a) temperature distribution, b) simulation on time for two positions y=0 (center of the line) and β=1.7 (periphery).

The Figure 13 allows a comparison of the treatment originated from the solid region and from the melted regions. We can see that the two curves penetrate the crystallization domain after a similar incubation time. However, in real time, the first one starts in front of the beam at a distance 3.4w from its center, that is before the temperature maximum whereas the second starts 1.7w after the

 doi:10.20944/preprints202404.1590.v1

temperature maximum. Consequently, the thermal treatment curve for the periphery is penetrating the crystallization domain before the one for the center. The periphery is thus in situation to stimulate the nucleation of the melted region. In addition, as both of treatment curves have almost no oscillations, the efficiency is obviously 100%.

Let us examine now, the effect of the scanning speed as reported in [10]. A large variation of the width of the crystallization region was found (by a factor 3), whereas the speed varied by a factor 5. The origin of this variation is not arising mainly from the time shift of the treatment curves with the speed as we can see in Figure 5. The effect is quite small. Another possibility could be from the pulse number received punctually and that could be smaller than the quantity for reaching the steady state. The steady state is reached after N_{ss} = 7.6 10^4 pulses (from Eq. A4 Appendix 1), whereas the number of pulses received punctually *Np* is 1.2 10^4 pulses for v=15 μm/s. However, for v=75 μm/s, *Np*=2400, which is significantly lower than N_{ss} (>30 times less). Consequently, the steady-state situation is not reached at those speeds. On the other hand, we can see from Figure 2 that the width at the beginning of the irradiation is like for (R_τ large, separated pulse contribution) and increases in the course of irradiation due to heat accumulation. To compute the width in the transitory stage, we assume here, that $T(r_{wdg}^0)$ crosses *Tg* for r_{wdg}^0>2. The use of T_{mean} is thus a good approximation. We have therefore to solve the equation below, for deducing r_{wdg}^0 according to the number of pulses. It reads (from Eq. A8 Appendix 4):

$$\bar{T}\left(r_{wdg}^0, R\tau, N\right) = \frac{\sqrt{\pi}}{R_\tau . r_{wdg}^0} . \left[erf\left(r_{wdg}^0\right) - erf\left(\frac{r_{wd}^0}{\sqrt{1+N.R\tau}}\right)\right] = \frac{T_g}{T_{00}} \; with \; T_{00} = \frac{A.E_p}{\pi^{3/2}\rho C_p w^3}$$

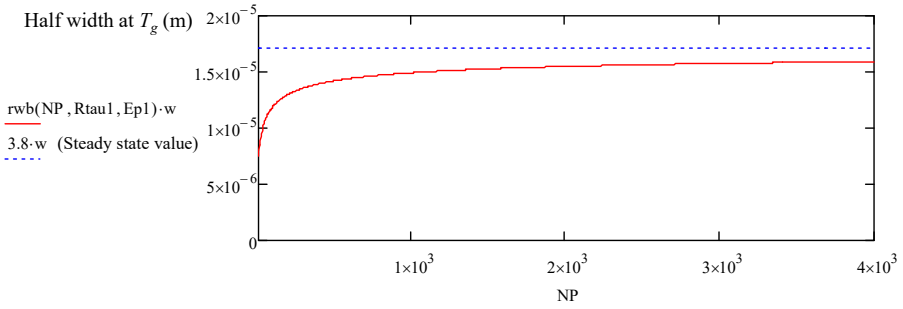

Figure 14. The half width variation during the transitory stage (*Np*<*Nss*). 3.8*w* is the maximum width (w=4.5 μm) for *Np*>*Ns* (at steady state), for *Ep*=4.2 μJ, R_τ=0.9.

The increase of the width, as a function of the pulse number is plotted in Figure 14. We see the broadening with the number of pulses that arises from heat accumulation as R_τ is around 1. But we find r_{wd}^0=3.5 for the speed in consideration, i.e. a decrease from 3.8, the value at the steady state. This does not account for variation by a factor 3. Even, if we consider the beginning of the irradiation, the possible variation would only be by a factor 2. On the contrary, results reported in [17] and used in Figure 11 are in agreement with this explanation (Laser parameters are: λ = 1030 nm; *RR* = 200 kHz; *NA* = 0.6; pulse duration = 250 fs). In that case, *Nss* is around 50 whereas *Np*>5280 for the speed lower than 125 μm/s. The steady state is always reached and the width is weakly varying as experimentally observed (the explanation is given about Figure 5).

The question is thus: is there other reasons to change the crystallization width? The difference between the beginning and the steady state could be the change of absorption due to the creation of defects in addition to the non-linear one, that play role of trapping centers of excited electrons produced by previous pulses. It is worth noticing that just a variation of *A* from 0.135 to 0.32 may explain that r_{wdg}^0 change from 1.6 to 3.8.

 doi:10.20944/preprints202404.1590.v1

On the other hand, it is observed in [10] that for a given pulse energy above some speed, the crystallization is only solid to solid transformation. This means according to the calculation that T_{max} is no more overcoming T_m. This is in agreement with lower absorption at larger speed. Furthermore, the observation of the shift of this turning point (called here v_t) with the pulse energy leads to consider that a particular dose D_0 is necessary for the absorption increase and for A to reach the value at the steady state. We would have therefore, the following relation: $Ep.2w.RR/v_t=D_0$. So, it would be possible to have an increase of temperature disconnected from the heat accumulation but arising from an increase of absorption related to defect creation.

Finally, from the Table 1, we can see that the steady state width of the crystallized region varies with the pulse energy for two reasons: because the beam waist increases with Ep and because the temperature distribution expends relatively with the beam waist because R_τ decreases and the interaction is thus more and more sensitive to heat accumulation and also because A increases on pulse energy.

Table 1. sum up of experimental and computed width according to the pulse energy.

E_p(µJ)	Pulse duration τ_p (fs)	w(µm)	A	R_τ	r_w(crystal) computed	r_w(crystal) experimental	r_w(melt) computed	r_w(melt) experimental	ref
0.5	300	1.23	0.035	7.9	1	uk	na	na	This work
0.7	300	1.65	0.09	4.4	1.05	1.00	na	na	[4]
1	300	2.23	0.12	2.4	1.18	uk	na	na	This work
1.3	300	2.6	0.15	1.8	1.47	1.6	0.48	1.1	This work
1.8	300	3.0	0.2	1.3	2.29	1.86	1.02	uk	[4]
4.2	175	4.5	0.32	0.9	3.79	3.50	1.71	uk	[19]

N.B.: na means not applicable and uk means unknown.

7. Discussion

Considering laser-induced crystallization, analytical formula can be used to compute the temperature oscillations in time when the steady is reached. These oscillations are limited between a maximum and minimum temperature, whatever the laser parameters and material properties, and established in the frame of a spherically symmetric energy source [13]. The broadening effect when increasing the pulse energy or the pulse density (inversely proportional to the beam scanning speed) was simulated.

We have shown previously how the spatial distribution and specifically its FWHM is changing during the transitory to a steady state depending on the ratio between the pulse period and the heat diffusion time (defined as R_τ). On the other hand, the temperature magnitude is defined by the beam waist and the fraction of absorbed incident energy (A). We show that when applied to real case and

 doi:10.20944/preprints202404.1590.v1

reliable simulation is requested, it is necessary to consider 1) an increase of the beam waist (w) with the pulse energy, and 2) the increase of the A factor with the pulse energy and the pulse duration. Such constraints that originate from non-linear effect in the solid, can only be extracted at the moment mainly from the experimental results available in literature (see Appendix 1 and 2) as mechanisms in the case of fs laser absorption are not clear enough for a robust simulation.

In such a way, within the approximation we used, we can deduce the following:

1 - The crystallization management is facilitated in a heat accumulation regime (R_t<<10). This allows the temperature oscillations to be quite small compared to average temperature values, thus, the laser parameters (i.e. Ep, R) can be easily adjusted to be completely above the T_g and below T_m during the thermal treatment time that is starting when the temperature is overcoming T_g. We were thus able to deduce thermal treatment curves. The scanning speed is also straightforward for the thermal curve to efficiently penetrate the crystallization domain. The crystallization process will originate from a solid-solid transition, and the width of the crystallized area is close to the beam waist. For the inorganic oxides, the thermal diffusivity is usually around 10^{-6} m^2/s (within a factor 2) so the diffusion time from a source with a beam waist of 1 μm is around < 0.5 μs. We are in the above conditions when the repetition rate frequency is much larger than 0.4-0.2 Mhz. However, if the focusing is not so tight, let say w = 2 μm, the heat diffusion time is four times larger and reaches 1-2 μs. So, the repetition rate has to be much larger than 5-10 MHz. However, in organic materials for which the diffusion time is 10 – 20 times longer, the heat accumulation regime is more easily reached and the thermal width more easily predictable.

If, the pulse energy is increased such that the temperature is overcoming the melting temperature around the center of the written line, the process changes, the starting time of the incubation is no more when the temperature overcomes T_g but when T decreasing below T_m as the process is a liquid to solid transformation. The crystallization domain is penetrated from the growth side renders the process sensitive to external stimulation, in particular to crystallization induction from the periphery where the temperature does not overcome Tm. As departing from the center and the temperature maximum of the treatment curve decreasing below T_m, a solid to solid transformation is occuring again. There are two regions in the crystallized line. It is shown that the solid to solid transformation region crystallizes sooner than the melted one and thus are source of nucleation for the melted one. The size of the crystallized region overcomes largely the beam waist in that case. The texture orientation of the line (if any) is thus defined by the peripheral region out of the beam and so defined mainly by the temperature gradient orientation. The large broadening with the pulse energy is defined in this case mainly by the pedestal of the temperature distribution (which follows a hyperbolic shape ($T \sim 1/r_w$) although beam waist and absorption fraction gives rise also to a broadening contribution. We pointed out also a unexpected result: the stimulation of heat accumulation regime on pulse energy increase and not only on RR.

2 - On the opposite, when heat accumulation is small or negligible (R_t>10, small RR, large diffusion time), the above processes are the same according to the pulse energy but the temperature oscillates largely in proportion. It results that just a small part of the oscillation is efficient (a few % or tens). This contributes to decrease proportionally the scanning speed in addition to the repetition rate that could be here smaller.

However, the weak efficiency for growth rate and a moderate pulse energy allows to penetrate the crystallization on the growth limited side of the crystallization domain and may allow to produce independent nanocrystals that have been revealed to be orientable with the laser polarization in the case of LNS glasses [20].

3 - We pointed out that the absorption may increase in the course of the irradiation and produce a large increase of temperature changing the crystallization process (from solid/solid to liquid/solid). This effect could be dose dependent (D_0=E_p.2w.RR/v_t) and leads to a transition speed v_t varying with the pulse energy. We suggest that this phenomenon arises from defects formation more easily to ionize.

8. Conclusions

 doi:10.20944/preprints202404.1590.v1

Using analytical formula computed from very simplified approximations (spherical approximation), we show that it is possible to use them for simulating crystallization processes by irradiation with a fs laser. However, for obtaining compatible results, the beam waist and the light absorption fraction have to be approximately known beside the physico-chemical data of the glass. After that, management of the crystallization process and the width of the crystallization line can be achieved according to pulse energy e.g. crystallite size, and also the effect of the scanning speed can be understood. For example, using the example of LNS glass, we show, in particular, that the crystallization process may changes with the scanning speed.

Lastly, the application of the temperature calculation can be extended to other processes depending on the temperature – distribution of the fictive temperature, viscoplastic effect (stress distribution), any chemical reaction that is thermally activated, chemical migration or the maximum energy not erasing type X or type II modification or luminescent defects creation or decomposition temperature of organic material. This management shall be even more accurate when fs laser is applied to organic matter in order to avoid complete material decomposition.

Author Contributions: Conceptualization, B.P.; funding acquisition, M.L.; investigation, R.Q. and B.P.; methodology, B.P.; project administration, B.P. and M.L.; resources, M.L.; supervision, B.P.; validation, R.Q.; visualization, M.C.; writing—original draft, B.P.; writing—review and editing, R.Q., B.P., M.C. and M.L. All authors have read and agreed to the published version of the manuscript.

Funding: This research was funded by Agence Nationale de la Recherche (ANR), FLAG-IR Project, award number ANR-18-CE08-0004-01, and REFRACTEMP project, award number ANR-22-CE08-0001-01. R.Q. acknowledges the China Scholarship Council (CSC) for the funding No. 201808440317 of her PhD fellowship.

Data Availability Statement: Data is contained within the article.

Conflicts of Interest: The authors declare no conflicts of interest.

Appendix 1 The Beam Width from the Literature and from Our Experiments

For that, we used the width of modification lines achieved by non thermal effect. The most obvious one is the line width of type II nanogratings as their structure is achieved only by the laser light whatever the material chemical composition.

We can first consider the beam focused with a length with NA and the effect of self-focusing. The formula for effective width at the focus in the material is given by Marburger et al. [21], Ashcom et al. [22] and Schaffer et al. [23] but their formula below does not take into account the defocusing effect due to the electron excitation. The defocusing effect is dependent of the excited electron density during the pulse and thus a too short lifetime or a weak pulse energy in the excited state of the electron may lead to the absence of this effect. The effective beam waist radius is given below:

$w_{eff} = \sqrt{\frac{\lambda^2/0.9\pi}{\frac{2\pi NA^2}{1-NA^2}\frac{I}{P_{cr}}\lambda^2}}$ with $P_{cr} = \frac{3.77\lambda^2}{8\pi n_0 n_2}$ n_2 being the non linear refractive index (3.2 10^{-16} cm^2/W [24,25]), n_0 the relative one, I the light intensity.

We can see that increasing the pulse energy, the intensity increases and thus the width decreases due to non-linear effects. It is the contrary of what it is observed in the case of laser leading to electron excitations [26].

In Lei et al. ([27],), the width increases with the energy above 0.2 µJ although the electron density is of the order of 0.01 excited electrons.nm^{-3}. Even for 0.1 excited electrons.nm^{-3}, it is said that there is a weak defocusing effect and the half width is 0.4 µm. However, without defocusing effect, the width should decrease on pulse energy increase.

These results and others are collected in table below

Table A1. some half width according to pulse energy, numerical aperture, and materials.

Wavelength (nm)	Pulse energy (µJ)	NA	Half width (µm)	Material	ref

 doi:10.20944/preprints202404.1590.v1

1030	0.1	0.6	0.31	silica	Ashcom et al. [28]
1030	0.5	0.6	0.24	silica	idem
1030	1	0.6	0.1	silica	idem
1030	0.19	0.3	0.4	silica	Lei et al. To be published in LPR Figure S2
1030	0.55	0.3	1.25	silica	idem
1025	0.7	Not known	1.		Beresna et al. [29] (in air) Figure 4
1030	1	0.6	2	silica	Qiong et al. [30]
1030	0.5	0.6	1.3	G1?	idem
1030		0.6	0.7	B33	idem
1030		0.6	1.65	ULE	idem
1030	3	0.6	2.1	ULE	idem
1030	1	0.6	1.25	BGG-ZnO	idem
1030	2	0.6	2.25	BGG-ZnO	idem
1030	0.7	0.6	1.65	LNS	Cao et al. [4]
1030	1.3	0.6	2.6	LNS	Cao et al. [4]
1030	0.5	0.6	1.6	LNSB	Muzi et al. [17]
1030	0.2	0.6	0.5	Suprasil	Our work
1030	5	0.6	5	Suprasil	Our work
1030	0.15	0.6	0.45	Suprasil	Our work
1030	2	0.6	1.75	Suprasil	Our work
800	0.18	1.35	0.4	glasses	Gamaly et al.[31] Figure 3
1030	0.8	0.6	2	Zn BGG	Yao et al. [32] Figure 2
1030	0.19	0.3	0.4	silica	[33] Figure S2

 doi:10.20944/preprints202404.1590.v1

1030	0.34	0.23	0.65	silica	[33] Figure S2
1030	0.55	0.16	2.2	silica	[33] Figure S2

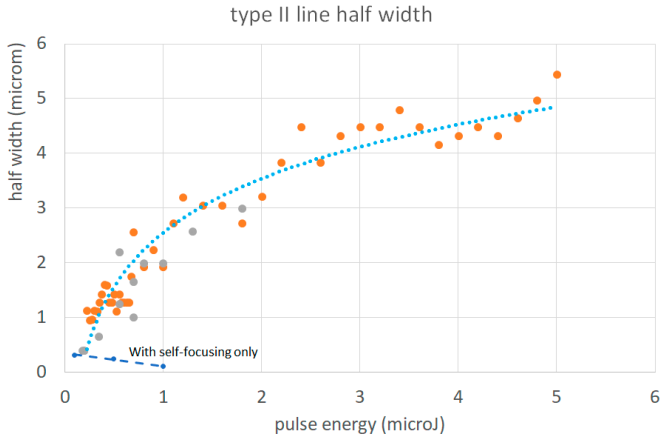

Figure A1. the half beam width according to the pulse energy from table A1 for various compounds, λ=NIR, various NA, often at the steady state.

Appendix 2 Fraction of Absorbed Beam Energy

The incident beam intensity from the laser is a parameter that is dependent of the material properties as well as the beam propagation especially on the focusing strength. Indeed, for working in volume, materials do not absorb linearly but non-linearly with an exponent of the intensity light that depends on the materials and on the pulse duration because it depends on the excited electron density that occurs in the few 10s fs [6]. The fraction of incident light absorbed is thus dependent on the intensity at the focus and around (before and after). In addition, the excited electron density may behave like a mirror and reflect a part of the incident intensity [34]. Moreover, for largest incident power, the excited electron density may have a defocusing effect that decrease the intensity and thus the non-linear absorption [26]. All of these processes are intricated and complex and leads to difficult prediction without heavy computations. As we need an estimate of this quantity for our computation, we have collected various results in the table below.

Table A2. fraction of absorbed energy according to pulse energy, pulse duration, numerical aperture of the focusing lens, and materials.

Wavelength (nm)	Pulse energy (μJ)	Pulse duration (fs)	NA	fraction	material	ref
800	0.1-0.7	50	0.5	0.2	silica	Couairon et al. [35]
800	1	90	Not mentioned	0.35	silica	Wu et al. [36]
800	2	90	Not mentioned	0.45	silica	Wu et al. [36]

 doi:10.20944/preprints202404.1590.v1

800	3	90	Not mentioned	0.54	silica	Wu et al. [36]
800	0.06-0.12	100	Not mentioned	<0.12	Metallic surface	Meng et al. 2023 Materials Surface métallique
800	0.25	100	Not mentioned	0.25	silica	Zhang et al. [37]
800	1/7.4	100	Not mentioned	<0.1	silica	Zhang et al. [37]
1026	4.2	175		0.58	silica	Computed from Veenhuisen et al. [10] see text
1030	0.6	190	0.16	0.25	silica	Wang et al. [38]
1030	1	190	0.16	0.36	silica	Wang et al. [38]
1030	0.2	300	0.3	0.04 to 0.06	Silica from 1 to 30 pulses	Lei et al. [39]
1030	0.6	300	0.16	0.05	silica	Wang et al. [38]
1030	0.69	300	0.16	<0.15	silica	Wang et al. [38]
1030	1	300	0.16	0.25	silica	Wang et al. [38]
1030	0.5	300	0.6	0.035	LNS	This work
1030	0.7	300	0.6	0.09	LNS	This work
1030	1.3	300	0.6	0.16	LNS	This work
1030	1.8	300	0.6	0.2	LNS	This work
1026	4.2	175	0.6	0.32	LNS	This work
1030	0.7	500	0.16	0.15	silica	Wang et al. [38]
1030	1	500	0.16	0.19	silica	Wang et al. [38]
1030	1	700	0.16	0.1	silica	Wang et al. [38]
1030	0.1	800	0.6	0.15	LNSB-Eu	Ari et al.[40]Figure 5a
1030	0.5	800	0.6	0.22	LNSB-Eu	Ari et al.[40]Figure 5a
1030	1.2	800	0.6	0.24	LNSB-Eu	Ari et al.[40]Figure 5a

 doi:10.20944/preprints202404.1590.v1

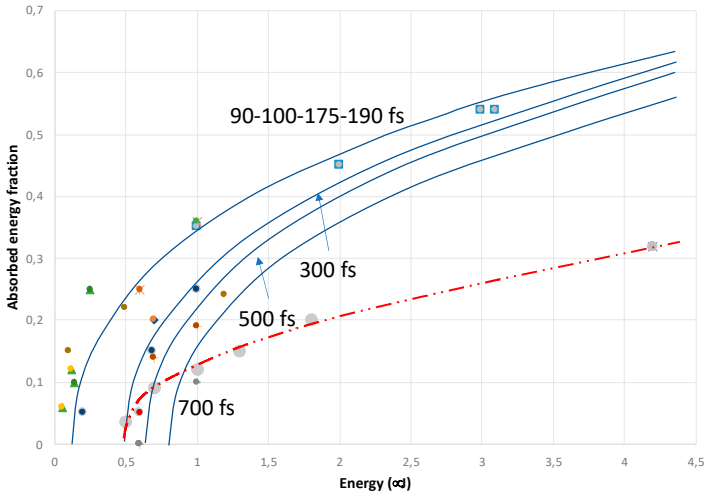

Figure A2. Plot of the absorbed energy fraction versus the pulse energy according to pulse duration (fs). The colors of the points make reference to the table A2: the blue curves is for silica and the red one for LNS glasses. However, lines are just guides for the eyes.

The absorbed energy fraction is very sensitive to the pulse duration for < 3,7microJ but less above (Zhang et al. [37])

Appendix 3

Table A3. physico-chemical and laser parameters.

	LNS glass : $33Li_2O$-$33Nb_2O_5$-$34SiO_2$ (mol %)	ref
specific density (ρ, kg/m³)	3830	Interpolated between SiO_2 and $NbLiO_3$.
Heat capacity (J/kg)	650	[41]
$K=D_{th}.\rho.C_p$ (J/K.m.s)	2.65	Computed from diffusivity
D_{th} (m²/s)	$9.1\ 10^{-7}$	[42,43]
Tg (°C)	579	[44,45]
Tm (°C)	1257	[44,45]

 doi:10.20944/preprints202404.1590.v1

Appendix 4

After reaching the steady state (the number of pulses for that is given in Table 3 of [13]), the expressions of the temperature maximum, minimum and oscillations are:

$$T_{max}(r_w, R_\tau) = \frac{exp\left[-\frac{(r_w)^2}{1+x_m \cdot R_\tau}\right]}{[1+x_m \cdot R_\tau]^{\frac{3}{2}}} + \frac{exp\left[-\frac{(r_w)^2}{1+(1+x_m)\cdot R_\tau}\right]}{2[1+(1+x_m)\cdot R_\tau]^{\frac{3}{2}}} + \frac{\sqrt{\pi}}{R_\tau . r_w}\left\{erf\left[\frac{r_w}{\sqrt{[1+(1+x_m)\cdot R_\tau]}}\right]\right\} \quad \text{Eq. A 1}$$

With $x_m = \frac{\sqrt{R_\tau}\sqrt{9R_\tau+32(r_w)^2}-3R_\tau-8}{8R_\tau}$ with $r_w > \sqrt{\frac{3}{2}+\frac{2}{R_\tau}}$ (x_m limited to 1) or $x_m = 0$, when, $r_w < \sqrt{\frac{3}{2}+\frac{2}{R_\tau}}$ whatever R_τ or R_τ less than $\frac{2}{r_w{}^2-1.5}$ when $r_w{}^2 > 1.5$).

$$T_{osc}(r_w, R_\tau) \approx \frac{\exp\left[-\frac{(r_w)^2}{1+x_m . R_\tau}\right]}{[1+x_m . R_\tau]^{\frac{3}{2}}} + \frac{\sqrt{\pi}}{R_\tau . r_w}\left\{\mathrm{erf}\left[\frac{r_w}{\sqrt{[1+(1+x_m).R_\tau]}}\right]\right\} - \frac{\sqrt{\pi}}{R_\tau . r_w}\mathrm{erf}\left(\frac{r_w}{\sqrt{1+R_\tau}}\right) \quad \text{Eq. A 2}$$

$$T_{min}(r_w, R_\tau) = \frac{\exp\left[-\frac{(r_w)^2}{1+(1+x_m)\cdot R_\tau}\right]}{2[1+(1+x_m)\cdot R_\tau]^{\frac{3}{2}}} + \frac{\sqrt{\pi}}{R_\tau . r_w}\left\{\mathrm{erf}\left[\frac{r_w}{\sqrt{[1+R_\tau]}}\right]\right\} \quad \text{Eq. A 3}$$

$$N^r_{ssmax} > \frac{1}{R\tau}\left[\left(\frac{2}{R_\tau . \varepsilon . T_{max}(r_w,\infty)}\right)^2 - 1\right] \qquad N^r_{ssmin} > \frac{1}{R_\tau}\left[\left(\frac{2}{R_\tau . \varepsilon . T_{min}(r_w,\infty)}\right)^2 - 1\right] \quad \text{Eq. A 4}$$

$$T_{max}(r_w, R_\tau, N) \approx \frac{\exp\left[-\frac{(r_w)^2}{1+x_m \cdot R_\tau}\right]}{[1+x_m \cdot R_\tau]^{\frac{3}{2}}} + \frac{\exp\left[-\frac{(r_w)^2}{1+(1+x_m)\cdot R_\tau}\right]}{2[1+(1+x_m)\cdot R_\tau]^{\frac{3}{2}}} + \frac{\exp\left[-\frac{(r_w)^2}{1+(N-1+x_m)\cdot R_\tau}\right]}{2[1+(N-1+x_m)\cdot R_\tau]^{\frac{3}{2}}} + \frac{\sqrt{\pi}}{R_\tau \cdot r_w}\left\{erf\left[\frac{r_w}{\sqrt{[1+(1+x_m)\cdot R_\tau]}}\right] - erf\left[\frac{r_w}{\sqrt{[1+(N-1+x_m)\cdot R_\tau]}}\right]\right\} \quad \text{Eq. A 5}$$

When the mean T can be used $\overline{T}(r, N) = \frac{1}{\tau_{RR}}\int_{\substack{\text{pulse period}\\ \text{at N}}} T(r, t)\, dt$, the formula is even simpler to be used after reaching the steady state. τ_{RR} is the period = $1/RR$

$$\bar{T}(r_w, R_\tau, \infty) = \frac{\sqrt{\pi}}{R_\tau . r_w} erf(r_w) \qquad N^r_{ssm}(r_w) = \frac{1}{R_\tau}\left[\left(\frac{2.r_w}{\sqrt{\pi}.\varepsilon.\boldsymbol{erf}(r_w)}\right)^2 - 1\right] \quad \text{Eq. A 1 and Eq. A 2}$$

$$\bar{T}(r_w, R_\tau, N) = \frac{\sqrt{\pi}}{R_\tau . r_w}.\left[erf(r_w) - erf\left(\frac{r_w}{\sqrt{1+N.R_\tau}}\right)\right] \quad \text{Eq. A 3}$$

Formula built for the simulation of the temperature oscillations at the steady state:

$$SimpulseT(r_w, x, R_\tau, E_p) = [T_{min}(r_w, R_\tau) + T_{osc}{}'(r_w, x, R_\tau)].T_{00}(E_p) \quad \text{Eq. A 4}$$

*w*here $T_{osc}{}'(r_w, x, R_\tau)$ is just the function $T_{osc}(r_w, R_\tau)$ where x_m is replaced by x.

The maximum temperature induced by one pulse is $T_{00} = \frac{A \cdot E_p}{\pi^{\frac{3}{2}}\rho C_p w^3}$ with A the fraction of absorbed energy, ρ and C_p are the glass density and heat capacity, w the beam waist at 1/e and E_p the pulse energy. Eq. A 10

Note that the time is introduced in the formula by r_{wd} which is a "moving" r_w (as the beam is scanning) and in x by rendering it periodic i.e. in taking only the floating value of t.RR.

References

1. Komatsu T and Honma T 2013 Laser patterning and characterization of optical active crystals in glasses *Journal of Asian Ceramic Societies* **1** 9-16
2. Neuville D, Cormier L, Caurant D and Montagne L 2017 From glass to crystal. Nucleation, growth and phase separation: from research to applications: EDP Sciences)
3. Teng Y, Zhou J, Sharafudeen K, Zhou S, Miura K and Qiu J 2014 Space-selective crystallization of glass induced by femtosecond laser irradiation *Journal of Non-Crystalline Solids* **383** 91-6

4. Cao J, Lancry M, Brisset F, Mazerolles L, Saint-Martin R and Poumellec B 2019 Femtosecond Laser-Induced Crystallization in Glasses: Growth Dynamics for Orientable Nanostructure and Nanocrystallization *Crystal Growth & Design* **19** 2189-205
5. Que R 2022 Demonstration of anisotropy control of optical properties induced by IR fs laser irradiation in organic materials : birefringence, di-attenuation, SHG, photoluminescence.
6. Lancry M, Groothoff N, Poumellec B, Guizard S, Fedorov N and Canning J 2011 Time-resolved plasma measurements in Ge-doped silica exposed to infrared femtosecond laser *Physical Review B* **84**
7. Uhlmann D R 1972 A kinetic treatment of glass formation *Journal of Non-Crystalline Solids* **7** 337-48
8. Weinberg M C, Birnie D P and Shneidman V A 1997 Crystallization kinetics and the JMAK equation *Journal of Non-Crystalline Solids* **219** 89-99
9. Deubener J, Allix M, Davis M J, Duran A, Höche T, Honma T, Komatsu T, Krüger S, Mitra I, Müller R, Nakane S, Pascual M J, Schmelzer J W P, Zanotto E D and Zhou S 2018 Updated definition of glass-ceramics *Journal of Non-Crystalline Solids* **501** 3-10
10. Keith Veenhuizen, Sean McAnany D N, Bruce Aitken, Volkmar Dierolf1 & and Jain H 2017 Fabrication of graded index single crystal in glass *Sci. Rep. 7*,44327;
11. Vigouroux H 2012 Etude de vitrocéramiques optiques pour le doublement de fréquence In: *Sciences Chimiques,* (University Bordeaux: University of Bordeaux, France) p 278
12. Yinnon H and D.R. Uhlmann D R 1983 ed D.R. Uhlmann and N.J. Kreidl: Academic Press)
13. Que R, Lancry M and Poumellec B 2024 Usable Analytical Expressions for Temperature Distribution Induced by Ultrafast Laser Pulses in Dielectric Solids *Micromachines* **15** 196
14. Miyamoto I, Horn A, Gottmann J, Wortmann D and Yoshino F 2007 Fusion Welding of Glass Using Femtosecond Laser Pulses with High-repetition Rates *Journal of Laser Micro Nanoengineering* **2** 57-63
15. Beresna M, Gertus T, Tomašiūnas R, Misawa H and Juodkazis S 2008 Three-Dimensional Modeling of the Heat-Affected Zone in Laser Machining Applications *Laser Chemistry* **2008** 976205
16. Miyamoto I, Horn A and Gottmann J 2007 Local Melting of Glass Material and Its Application to Direct Fusion Welding by Ps-laser Pulses *Journal of Laser Micro Nanoengineering* **2** 7-14
17. Muzi E, Cavillon M, Lancry M, Brisset F, Que R, Pugliese D, Janner D and Poumellec B 2021 Towards a Rationalization of Ultrafast Laser-Induced Crystallization in Lithium Niobium Borosilicate Glasses: The Key Role of The Scanning Speed *Crystals* **11**
18. Bricchi E, Klappauf B G and Kazansky P G 2004 Form birefringence and negative index change created by femtosecond direct writing in transparent materials *Optics Letters* **29** 119-21
19. Cao J 2017 Creation and orientation of nano-crystals by femtosecond laser light for controlling optical non-linear response in silica-based glasses Création et orientation de nano-cristaux par irradiation laser femtoseconde pour le contrôle de l'orientation des propriétés optiques non-linéaires dans des verres à base de silice. Université Paris Saclay (COmUE))
20. Cao J, Matthieu L, François B and Bertrand P 2022 Orientable Nonlinear Optical Crystals and Periodic Nanostructure by Femtosecond Laser Irradiation *激光与光电子学进展* Laser & Optoelectronics Progress **59** 1516001
21. Marburger J H 1975 Self-focusing: Theory *Progress in Quantum Electronics* **4, Part 1** 35-110
22. Ashcom J B, Gattass R R, Schaffer C B and Mazur E 2006 Numerical aperture dependence of damage and supercontinuum generation from femtosecond laser pulses in bulk fused silica *J. Opt. Soc. Am. B* **23** 2317-22
23. Schaffer C B, Brodeur A and Mazur E 2001 Laser-induced breakdown and damage in bulk transparent materials induced by tightly focused femtosecond laser pulses *Measurement Science and Technology* **12** 1784
24. Kato T, Suetsugu Y and Nishimura M 1995 Estimation of non-linear refractive index in various silica-based glasses for optical fibers. *Optics Letters* **20** 2279-81
25. Le Boiteux S, Segonds P, Canioni L, Sarger L, Cardinal T, Duchesne C, Fargin E and Le Flem G 1997 Nonlinear optical properties for TiO_2 containing phosphate, borophosphate, and silicate glasses. *Journal of Applied Physics* **81** 1481-7
26. Couairon A and Mysyrowicz A 2007 Femtosecond filamentation in transparent media *Physics Reports* **441** 47-189
27. Lei Y 2023 Laser Modification of Materials at Micro- and Nanoscale for Photonics and Information Technology. In: *ORC*: Southampton)
28. Ashcom J B, Gatlass R R, CSchaffer C B and Mazur E 2006 Numerical aperture dependence of damage and supercontinuum generation from femtosecond laser pulses in bulk fused silica. *Journal of Optical Society of America B* **23** 2317-22
29. Beresna M, Kazansky P G, Svirko Y, Barkauskas M and Danielius R 2009 High average power second harmonic generation in air *Applied Physics Letters* **95** 121502
30. Xie Q, Cavillon M, Pugliese D, Janner D, Poumellec B and Lancry M 2022 On the Formation of Nanogratings in Commercial Oxide Glasses by Femtosecond Laser Direct Writing *Nanomaterials* **12**

 doi:10.20944/preprints202404.1590.v1

31. Gamaly E G, Juodkazis S, Nishimura K, Misawa H, Luther-Davies B, Hallo L, Nicolai P and Tikhonchuk V T 2006 Laser-matter interaction in the bulk of a transparent solid: Confined microexplosion and void formation *Physical Review B* **73** 214101
32. Zaiter R, Lancry M, Fargues A, Adamietz F, Dussauze M, Rodriguez V, Poumellec B and Cardinal T 2023 Optical and structural characterization of femtosecond laser written micro-structures in germanate glass *Scientific Reports* **13** 11050
33. Wang H, Lei Y, Shayeganrad G, Svirko Y and Kazansky P G 2024 Increasing Efficiency of Ultrafast Laser Writing Via Nonlocality of Light-Matter Interaction *Laser & Photonics Reviews* **n/a** 2301143
34. Garcia-Lechuga M, Haahr-Lillevang L, Siegel J, Balling P, Guizard S and Solis J 2017 Simultaneous time-space resolved reflectivity and interferometric measurements of dielectrics excited with femtosecond laser pulses *Physical Review B* **95** 214114
35. Couairon A, Sudrie L, Franco M, Prade B and Mysyrowicz A 2005 Filamentation and damage in fused silica induced by tightly focused femtosecond laser pulses *Physical Review B* **71** 125435
36. Wu A Q, Chowdhury I H and Xu X 2005 Femtosecond laser absorption in fused silica: Numerical and experimental investigation *Physical Review B* **72** 085128
37. Zhang S, Menoni C, Gruzdev V and Chowdhury E 2022 Ultrafast Laser Material Damage Simulation—A New Look at an Old Problem. In: *Nanomaterials,*
38. Wang H, Lei Y, Wang L, Sakakura M, Yu Y, Shayeganrad G and Kazansky P G 2022 100-Layer Error-Free 5D Optical Data Storage by Ultrafast Laser Nanostructuring in Glass *Laser & Photonics Reviews* **16** 2100563
39. Lei Y, Shayeganrad G, Wang H, Sakakura M, Yu Y, Wang L, Kliukin D, Skuja L, Svirko Y and Kazansky P G 2023 Efficient ultrafast laser writing with elliptical polarization *Light: Science & Applications* **12** 74
40. Ari J, Cavillon M, Lancry M and Poumellec B 2023 Polarization-dependent orientation of LiNbO3:Eu3+ nanocrystals using ultrashort laser pulses in borosilicate glasses *Advanced Optical Technologies* **12**
41. Company I C C 1927 *Chemical Engineering Catalog* vol Twelfth Annual Edition (New York, USA: The Chemical Catalog Company, Inc.)
42. Kingery W D 1955 Thermal Conductivity: XII, Temperature Dependence of Conductivity for Single-Phase Ceramics *Journal of the American Ceramic Society* **38** 251-5
43. Morgan R A, Kang K I, Hsu C C, Koliopoulos C L and Peyghambarian N 1987 Measurement of the thermal diffusivity of nonlinear anisotropic crystals using optical interferometry *Appl. Opt.* **26** 5266-71
44. Sigaev V N, Golubev N V, Stefanovich S Y, Komatsu T, Benino Y, Pernice P, Aronne A, Fanelli E, Champagnon B, Califano V, Vouagner D, Konstantinova T E and Glazunova V A 2008 Second-order optical non-linearity initiated in Li2O–Nb2O5–SiO2 and Li2O–ZnO–Nb2O5–SiO2 glasses by formation of polar and centrosymmetric nanostructures *Journal of Non-Crystalline Solids* **354** 873-81
45. Shimada M, Honma T and Komatsu T 2018 Laser patterning of oriented LiNbO3 crystal particle arrays in NiO-doped lithium niobium silicate glasses *International Journal of Applied Glass Science* **9** 518-29